On Predicting Transitions to Compliant Surfaces in Adults with Transtibial Amputation: A Real-Time Classification Approach

Charikleia Angelidou, Jaclyn M. Sions and Panagiotis Artemiadis*, *IEEE Senior Member*

***Abstract*— Walking on compliant surfaces, such as carpets, grass, and soil, presents a unique challenge, particularly for those relying on prosthetic interventions. Ensuring the safety, stability, and fluidity of movement on these surfaces is paramount to prevent falls and related balance issues in this population. This study presents the first attempt to classify and predict surface compliance in individuals with transtibial lower-limb amputations. By integrating electromyographic (EMG), kinematic, and kinetic data, our system effectively distinguishes user intent across varying surface stiffnesses representing diverse real-world terrains. As we demonstrate the algorithm's success within a clinical population, we achieve up to 83% prediction accuracy, attaining comparable results as in previously tested healthy populations. The suggested framework is a critical component for high-level controllers for advanced prostheses and it holds potential for real-time integration, enabling adaptive adjustments to the prosthetic device in response to both user intent and environmental stimuli.**

I. Introduction

Given the significance and prevalence of walking in daily living, comprehending and modeling gait is essential. Even in a controlled setting with level, rigid ground, and no external disturbances, gait modeling is intricate and does not fully capture the complexities of real-world movement [1]. To devise effective rehabilitation strategies for paretic gait and advanced controllers for prosthetic and wearable technologies, we must understand and model gait control across diverse environments, such as uneven and soft surfaces. Walking on compliant terrain specifically presents a unique challenge and is a critical aspect of daily mobility for many individuals. Unlike walking on rigid, stable surfaces, compliant terrains can shift underfoot and disrupt normal movement dynamics, thus requiring greater effort, balance, and coordination [2–4].

Understanding the dynamics of walking on these surfaces is particularly crucial for those with mobility impairments, such as individuals with lower limb amputation (LLA), who often find navigating these terrains much more difficult [5]. Walking stability and agility on non-flat and compliant surfaces pose a significant challenge, particularly for this population, primarily due to the lack of distal muscles and sensory feedback from the lower limb, as well as the lack of intuitive control of the mechanical impedance of the prosthesis [6]. Relevant works focusing on LLA populations specifically report lower walking speeds and increased step width, step time asymmetry, and variability for individuals with transfemoral amputation on compliant terrains [7], as well as decreased postural stability for those with transtibial amputation when standing on a compliant foam surface [8].

Despite the urgent need to understand and enhance mobility on compliant surfaces for this population, research in this area is limited. Specifically, research on controllers for compliant terrains has made significant advances primarily in legged robots, especially bipedal and monopod systems. Techniques such as model predictive and impedance control have enabled robots to adapt to soft and uneven terrains [9]. However, studies for advancing prosthetic limbs and wearable devices over compliant terrains, remain limited and focus on a restricted number of study variables [10, 11] or on isolated patient populations [12]. Further research is therefore needed to develop prosthetic and wearable device controllers for real-world conditions, where uneven and compliant terrains pose significant challenges to clinical populations.

To address this gap, a few works have delved deeper into the effects of compliant terrains, thoroughly studying walking stability [13], muscle activations and gait kinematics [14–16]. Some of our recent works also propose an intelligent control framework for achieving dynamic locomotion across various compliant surfaces [17–19]. The proposed intelligent system encompasses a multi-level controller for robotic ankle-foot prostheses that interacts with the human user and the environment. The control architecture includes a 1) high-level anticipatory control module aimed at predicting user intent to step on a dynamic surface before contact with the ground by classifying surface compliance using electromyographic (EMG), kinematic, and kinetic data from the user and a 2) reactive control module aimed at directly aiding the tuning of the lower-limb prostheses' high-level control during stepping on grounds with different profiles and compliances. The overall concept of the proposed system is shown in Fig. 1.

Considering that the most challenging part of traversing compliant terrain is the first contact of the individual with the new surface, we primarily focus on the former mechanism that centers around the anticipation preceding the step onto a compliant surface. Building upon our previous studies, the goal of this paper is to adjust and evaluate the proposed framework with individuals with LLA and analyze the anticipatory mechanisms during transitions to compliant

*This material is based upon work supported by the National Science Foundation under Grants No. 2020009, 2015786, 2025797, and 2018905.

Charikleia Angelidou and Panagiotis Artemiadis are with the Mechanical Engineering Department, at the University of Delaware, Newark, DE 19716, USA. cangelid@udel.edu, partem@udel.edu.

Jaclyn M. Sions is with the Department of Physical Therapy at the University of Delaware, Newark, DE 19716, USA. megsions@udel.edu.

*Corrresponding author

surfaces for this population. Unlike able-bodied participants, the application of this framework to individuals with LLA is quite different and more challenging. Specifically, selective muscle atrophy in people with LLA has been shown to affect the muscle volume of certain muscles [20], which may subsequently lead to changes in EMG signal strength, while the quality of the acquired EMG recordings is also highly dependent on the level of amputation of each individual, as well as the respective surgical intervention they have undergone.

To our knowledge, this is the first attempt to predict and classify surface compliance using biomechanical signals from individuals with a unilateral transtibial (TT) amputation. We expect that the proposed controller will advance the state-of-the-art of robotic prostheses by incorporating human-in-the-loop strategies and enable efficient and robust behavior in dynamic environments, ultimately improving the quality of life for individuals with gait impairments, including those with LLA.

II. METHODS

A. Participant Data

In order to investigate the efficiency of our prediction algorithm for the case of individuals with LLA, we recruited one participant with a unilateral TT amputation. The recruited TT participant is a reportedly active, community ambulator who utilizes their prostheses for a minimum of 12 hours daily. The participant did not report any nerve damage or sensation-related concerns, nor disclosed any comorbidities that would affect their participation in the study. Detailed information about the participant, the nature of the amputation, and the prosthetic componentry is provided in Table I. The participant provided written consent and the study protocol has been approved by the University of Delaware Institutional Review Board (IRB) under study ID# 1520622-8.

B. Variable Stiffness Treadmill 2 (VST 2)

The walking assessment was conducted using a unique robotic platform developed by our lab to simulate walking on soft surfaces called the Variable Stiffness Treadmill 2 (VST 2) [21], shown in Fig. 2. The VST 2 is capable of independently altering the stiffness of both belts within a range of 13 kN/m, which corresponds to the lowest surface stiffness that can be achieved by the treadmill, to 1.5 MN/m, which corresponds to rigid ground walking. The speed of the belts is also independent, as each belt has a dedicated motor. This treadmill setting captures the complexities of everyday walking by recreating compliant surface walking and reproducing real-world stiffness conditions in the lab.

C. Experimental Protocol

The study visit included three phases: 1) participant eligibility confirmation and preparation, 2) participant familiarization with the experimental equipment (VST 2), and 3) completion of 3 walking trials.

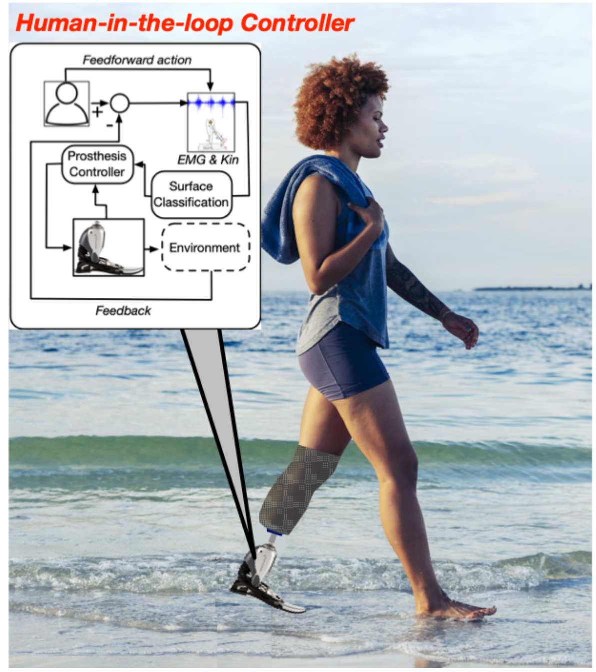

Fig. 1: Presentation of a robotic ankle-foot prosthesis that interacts with the human user and the environment. Overview of the human-prosthesis interface and the proposed research framework including the anticipatory and compensatory control modules.

Age	47
Cause of Amputation	Congenital Absence
Amputated Side	Left
Socket Type	Patellar Tendon Bearing (PTB)
Socket Material	Carbon/Epoxy-Acrylic/ Expandable
Foot Type/ Manufacturer	Ossur LP Variflex
K-level	K3

TABLE I: Participant features and prosthetic components.

1) Participant preparation: Upon arrival at the research laboratory, the participant was asked to sign an IRB-approved consent form. A licensed physical therapist (PT) was present in the room throughout the duration of the study to ensure the participant's safety and well-being. The PT also administered overground walking tests that were then used to determine an appropriate and comfortable treadmill speed for the participant. Following clearance from the PT, the participant was equipped with surface EMG electrodes and a set of lower-body motion capture markers.

Markers were placed at all required locations for the Vicon Plug-in Gait Lower Body model [22]. Lower body kinematics were recorded using a total of 20 reflective markers on the pelvis, thighs, shanks, and feet of the participant. Kinematic data was sampled at 100 Hz using the Vicon motion capture system. An 11-channel wireless surface EMG system (Trigno – Delsys, Massachusetts, USA), operating at 2000 Hz, recorded EMG signals from several lower limb muscles including the tibialis anterior (TA), soleus (SOL), gastrocnemius (GA), rectus femoris (RF), vastus lateralis (VL), vastus medialis (VM) and biceps femoris (BF) of both legs. For the prosthetic side, the TA, SOL, and GA muscle activities were not recorded, due to the inability to place the EMG electrodes within the prosthetic socket. Variability was reduced by following SENIAM guidelines [23, 24]. To prevent EMG sensor displacement during data acquisition, each sensor was secured with medical tape (see Fig. 2), ensuring reliable measurements without introducing errors. Muscles were contracted at each sensor placement to ensure that a viable location was found, and a low signal-noise ratio was retained. The participant wore a body weight support (BWS) harness throughout the whole duration of the experiment session. The BWS did not offset any weight and was exclusively used for safety purposes.

2) Participant familiarization: Before the start of each trial, we introduced the participant to the VST 2. At this time, no data was recorded. The acclimation phase of the study consisted of a single trial, where the participant was introduced to walking over rigid ground (R), as well as three different levels of surface stiffness that were labeled from less to most compliant as high (S_H), medium (S_M), and low (S_L) stiffness surfaces. The trial lasted a few gait cycles per stiffness condition to avoid fatigue before the start of the experiment. The average vertical belt deflection for S_H was approximately $d_H = 1cm$, while for S_M and S_L to be $d_M = 2cm$ and $d_L = 3cm$ respectively. The goal of selecting three stiffness levels was to simulate a range of real-world ambulation environments, such as balancing on a soft yoga mat, traversing a muddy path, or enjoying a walk on a sandy beach. The selection of the stiffness levels was done to ensure that the tested stiffness conditions were noticeably different by the participant. During the acclimation phase and following the PT-administered overground walking tests, a comfortable walking speed of 0.7 m/s was selected. It must be noted that the specific properties of our instrumented treadmill platform made the comfortable speed selection lower than the recorded overground speed (1.2 m/s).

3) VST 2 Walking trials: The general outline of the experimental protocol is demonstrated in Fig. 2. The right (intact) side of the VST 2 remained rigid for the entire duration of the experiments, while expected stiffness changes were applied unilaterally to the left (prosthetic) side. The stiffness perturbations were introduced at regular intervals, ranging between 3 to 5 consecutive rigid gait cycles. The timing of each perturbation was coordinated to ensure that, during a compliant gait cycle, the prosthetic leg consistently encountered a walking surface with a high, medium, or low stiffness accordingly. The change in the stiffness of one belt was based on the assumption that transitions between surfaces in everyday life activities are first experienced by one leg. A monitor setup located in front of the VST 2 provided a visual cue, synchronized with the participant's gait, and notified them about an upcoming stiffness change. With every completed gait cycle, a colored patch (different color for every stiffness condition) would specifically move from the top toward the bottom of the screen. The bottom of the screen corresponded to the participant's current step, so whenever the colored patch reached the bottom, the subjects knew that the upcoming step would take place on compliant ground, as well as the level of stiffness they would encounter

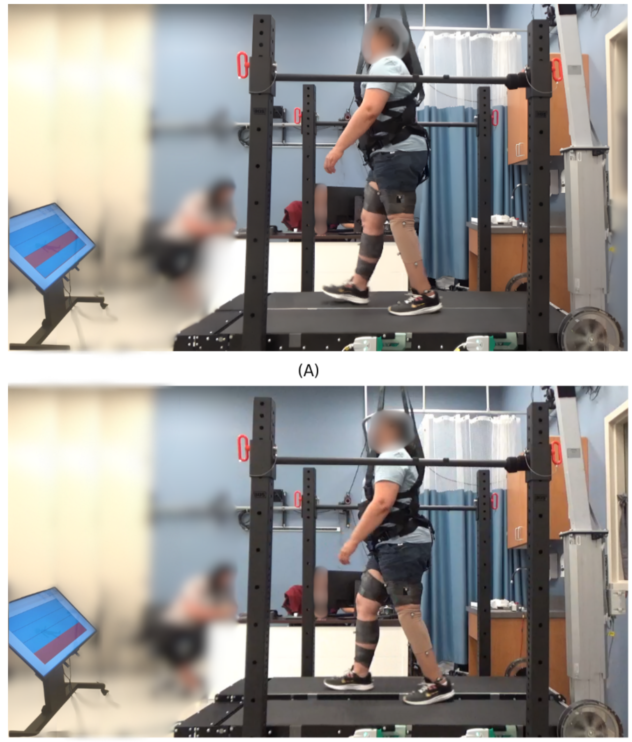

(A)

(B)

Fig. 2: Participant walking on the VST 2 platform during a trial. The left leg is the prosthetic side. Subject instrumentation is shown, including EMG electrodes and reflective motion capture markers. The experiment setup including a view of the VST 2 and the visual feedback monitor is presented. (A) Participant stepping on a rigid (R) surface, preparing to transition to a low stiffness (S_L) surface. Both VST 2 belts are set to rigid. (B) Participant stepping on a low-stiffness surface. The right VST 2 belt is set to rigid, while the left belt is set to compliant.

(see Fig. 2). Each trial always consisted of unilateral perturbations of a single stiffness level. Specifically, the first trial included S_L perturbations, the second trial S_H, and the third and final trial consisted of S_M perturbations. The participant was asked to walk for an average duration of 5 minutes per trial, which corresponded to a total of 245 gait cycles. To avoid fatigue, breaks of a minimum of 2 minutes were included between the trials.

During the treadmill session, the participant's heart rate was continuously monitored using a heart rate monitor (Polar H10) wrapped around their chest to ensure cardiovascular safety and to track any potential physiological stress. Additionally, the PT was monitoring the participant's physiological stress using the Borg Scale of Perceived Exertion, while also observing closely for other signs of distress. These precautions were taken to provide a controlled and safe environment for the participant while collecting reliable data on gait dynamics over varying terrain stiffness conditions for this population, which has not been tested before.

D. Data Processing

For each muscle, the raw EMG data was initially filtered using a fourth-order Butterworth band-pass filter with cut-off frequencies set at 30 Hz and 300 Hz. Following this, the data underwent full-wave rectification, and the linear envelope of each muscle signal was calculated using a moving average with a 200-point window. The data was then further processed with an additional fourth-order Butterworth low-pass filter. Next, to standardize the EMG data, the maximum voluntary contraction (MVC) value was calculated as the 99.9^{th} percentile value of each muscle activation across each trial.

Force data recorded at 65 Hz was processed with a moving average filter with a window size of 60 data points. For all trials performed on the treadmill, heel strike events were detected using the already processed force data. Specifically, once the measured filtered force on each belt of the treadmill increased to about 5% of the participant's body weight, this was defined as a heel-strike event. The raw kinematic, kinetic and EMG data were then segmented into gait cycles, with each cycle defined as beginning and ending at Left Heel Strike (LHS).

Since this work focuses on studying the anticipatory mechanisms involved in human locomotion before encountering a compliant surface, the gait cycles of interest pertain to transitions between surfaces. We define a transition as the rigid gait cycle preceding a stiffness change. The transition gait cycles are labeled as i) transition to high (TH), ii) transition to medium (TM), and iii) transition to low (TL) stiffness surface depending on the compliance of the upcoming step. All transitions were initiated on rigid ground (R) to ensure uniformity across the different conditions, while all gait cycles following a stiffness perturbation are excluded from any further analysis.

E. Classification and Prediction Framework

For the sake of brevity, only a brief description of the classification framework is provided in this work.

1) Continuous Overlapping Windows: The overlapping window technique is crucial for enhancing the accuracy and reliability of classification and prediction tasks, particularly in time-series data analysis. By allowing windows to overlap, this method ensures that each data point contributes to multiple windows, thereby capturing more contextual information and reducing the risk of missing critical transitions between states. This overlap improves the model's ability to detect subtle patterns and temporal dependencies, which are often essential for accurate predictions. Overlapping windows are especially effective as they also enable the detection of patterns at an earlier stage compared to other methods [25]. This characteristic of sliding windows renders them a suitable approach for our classification task, where predicting user intent promptly is of paramount importance to prevent balance-related falls in populations with transtibial amputation. We specifically applied a continuous sliding window technique to the EMG and kinematic signals of every gait cycle. The terminal stance (before left toe-off) and the swing phase (between left toe-off and left heel-strike) of each gait cycle were, in particular, segmented into 150 ms long windows with a 50% window overlap, resulting in six sliding windows. The kinetic (vertical Ground Reaction Force (vGRF)) data did not comply with the windowing segmentation, since vGRFs during the terminal stance and swing phases remain close to 0 due to the absence of immediate foot-ground contact, thus not offering any windows with usable information.

2) Feature Engineering for Gait Classification and Prediction: In this study, following the paradigm applied in our previous work [19], we did not exclude any muscles from the feature engineering process, allowing for an unbiased evaluation of each variable's impact on the final prediction. A total of 18 EMG and 3 kinematic (KIN) features were extracted from each EMG and KIN signal source per window. The EMG signal source specifically refers to each recorded muscle, while the KIN signal source refers to the Center of Mass (CoM) of the body, and the ankle, knee, and hip angular position, velocity and acceleration. This process produced a 249 feature long vector per segmented window ($\mathbf{f}$), comprising of 18 features from each of the 11 specified muscles, and 3 features from each of the 17 specified kinematic signal sources. The EMG features extracted from each muscle specifically included the Mean Absolute Value, Waveform Length, Difference Variance Value, Root Mean Square, Simple Square Integrated, Integrated EMG, Variance of EMG, Difference Absolute Mean Value, Standard Deviation, Average Amplitude Change, Kurtosis, Skewness, and 6th order Autoregression Coefficients. The KIN features extracted from each KIN signal source listed above included the maximum, mean, and minimum of the corresponding values within each segmented window.

For the incorporation of the kinetic data within the resulting feature vector $\mathbf{f}$, we extracted three characteristic vGRF curve points: the passive (1st) peak, corresponding to subject weight acceptance, the active (2nd) peak, corresponding to push-off, and the valley area forming between the two peaks. The extracted vGRF features ($\mathbf{f_{GRF}}$) were then temporally concatenated to the feature vector created for each of the segmented windows, resulting in a final feature vector of 252 features ($\mathbf{F}$) per segmented window $q = 1, \ldots, 6$.

$$\mathbf{F_q} = [\mathbf{f}, \mathbf{f_{GRF}}]_q \tag{1}$$

By identifying and retaining only the most relevant features, feature selection enhances model performance, improves interpretability, and reduces the risk of overfitting. We therefore employed Neighborhood Component Analysis (NCA) as an effective method for feature selection, as it reduces the dimensionality of the feature vector by selecting features that contribute most to the predictive power of the model. NCA optimizes a distance metric by learning a weighted transformation of the input features, thereby emphasizing those features that improve the classification accuracy. The NCA algorithm implementation was completed using the $fscnca$ Matlab command which uses the regularized objective function as introduced in [26].

3) k Nearest Neighbors (kNN) Algorithm: The kNN classification algorithm has been shown to reliably and accurately predict outcomes, making it the primary classification method selected for this study [17, 18]. The algorithm's

	Window 1		Window 2		Window 3		Window 4		Window 5		Window 6	
Metric	*Macro*	*Micro*	*Macro*	*Micro*	*Macro*	*Micro*	*Macro*	*Micro*	*Macro*	*Micro*	*Macro*	*Micro*
Precision	0.7516	-	0.70063	-	0.73197	-	0.77652	-	0.77687	-	0.72738	-
Recall	0.74405	-	0.69286	-	0.70595	-	0.76071	-	0.7619	-	0.70952	-
F1-Score	0.73759	0.74138	0.69564	0.68966	0.71419	0.7069	0.75685	0.75862	0.76178	0.75862	0.71215	0.7069

TABLE II: Macro and micro metrics for k-NN performance evaluation. In multi-class classification scenarios where each observation is assigned a single label, the micro-F1, micro-precision, and micro-recall metrics will yield identical values. This equivalence explains why we report only the micro F1-score value.

simplicity is particularly noteworthy, as it relies on straightforward comparisons to identify similar records in the training data, effectively generating accurate predictions. In this implementation, we used the Euclidean distance between a test and a training data point, coupled with an inverse distance weight, and $k = 9$ nearest neighbors. A distinct classifier was trained for each segmented window, resulting in a total of six separate classifiers and thus decisions per gait cycle.

4) Naive Bayes for Final Prediction: To determine the user's next step, it is necessary to integrate the individual decisions from the distinct classifiers into a conclusion about the stiffness of the forthcoming surface. To accomplish this, we utilized a Naive Bayes classifier, which combines the six separate decisions from the kNN window classifiers into a single final decision. Naive Bayes classification is a probabilistic algorithm grounded in Bayesian probability theory. The algorithm estimates the probability that a data point belongs to a particular class based on the probabilities of its individual features given that class [27]. Naive Bayes classifiers assign observations to the most likely class using the maximum a posteriori decision rule, where the algorithm estimates the density of the predictors within each class and models the posterior probabilities according to Bayes' rule for all $n = 1, \ldots, N$, as:

$$\hat{P}\left(Y = n | X_1, \ldots, X_P\right) = \frac{\pi(Y=n)\prod_{j=1}^{P} P(X_j \mid Y=n)}{\sum_{n=1}^{N} \pi(Y=n)\prod_{j=1}^{P} P(X_j \mid Y=n)} \tag{2}$$

, where Y is the random variable corresponding to the class index of an observation, $X_1, \ldots, X_P$ are the random predictors of an observation, and $\pi(n)$ is the prior probability that a class index is n. Building on the independent window decisions generated by the kNN classification, we sequentially applied the Naive Bayes classifier, starting with the decision from window 1, then incorporating decisions from windows 1 and 2, followed by windows 1, 2, and 3, and continuing this process until decisions from all windows were included. The objective of this method was to assess how early in the windowing process we could reach a final decision about the stiffness of the upcoming surface.

III. Results

A. Improved classification accuracy as participant nears the new surface

The results from each window classifier reveal that the prediction accuracy consistently improves toward the end of the gait cycle, particularly in the final segmented windows. Analysis of the participant data shows an increase in the Balanced Accuracy metric during windows 4 and 5, reaching

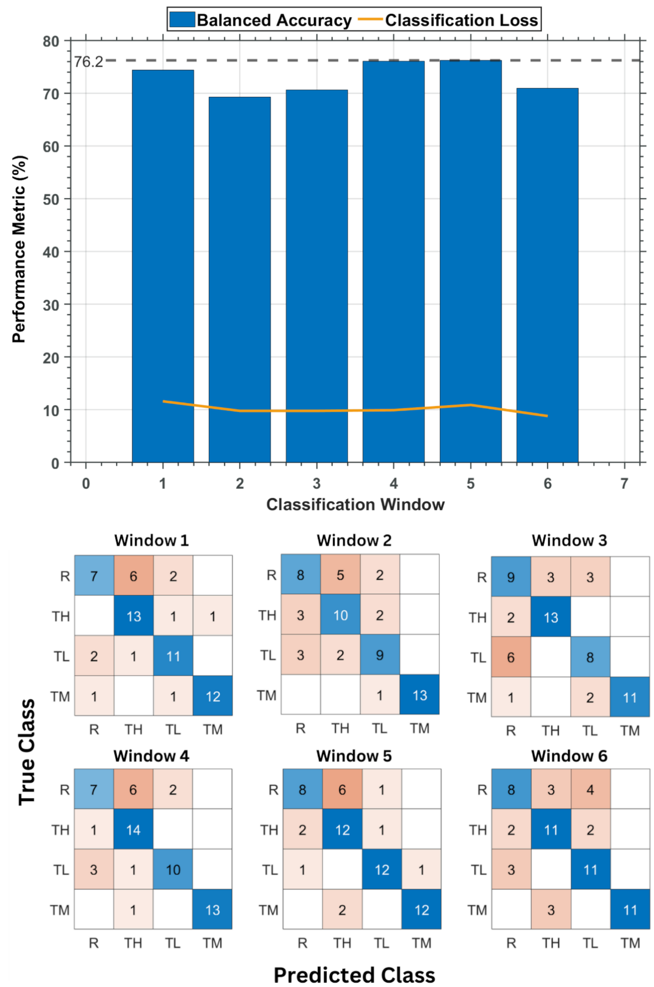

Fig. 3: Performance evaluation using the Balanced Accuracy and Classification Loss metrics (top) and the corresponding confusion matrices (bottom) for the TT participant using k-NN window-classifiers.

an accuracy of 76.2% (see Fig. 3). A similar peak can be also seen in the Macro F1-Score, Precision, and Recall metrics, mirroring the behavior of the accuracy metric (see Table II).

Analyzing the classification loss also serves as a valuable measure to assess the predictive error in classification models. This loss is derived from a cross-validated classification approach. For each fold, the classification loss is calculated on the validation fold using a model trained on the training fold. In our implementation, we determine the minimal expected misclassification cost based on the posterior probabilities from the kNN algorithm. The overall classification loss is computed as the weighted average of this minimal expected misclassification cost for observations $j = 1, \ldots, m$, represented by $L = \sum_{j=1}^{m} w_j u_j$. Here, u_j

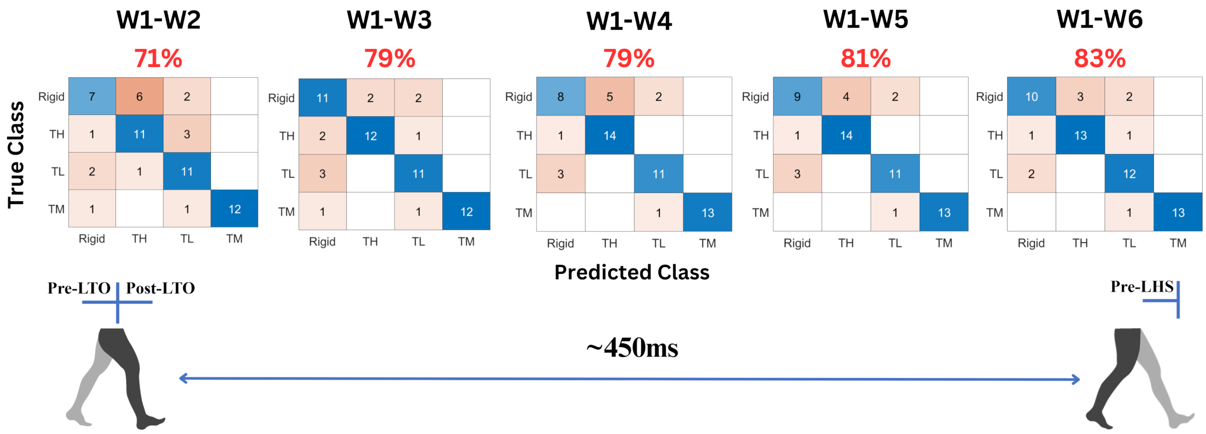

Fig. 4: Naive Bayes performance evaluation using confusion matrices from each window combination. The number of windows increases from left to right, with W1-W2 corresponding to the final prediction accuracy (denoted in red) after combining windows 1 and 2, W1-W3 corresponding to the final prediction accuracy after combining windows 1, 2, and 3, and so on. The earliest window combination (W1-W2) represents the late stance phase of gait (around left toe off - LTO), while the latest window combination (W1-W6) represents the late swing phase of gait (at left heel strike - LHS).

refers to the cost associated with making a prediction, and w_j is the weight for each observation j. Matlab ensures that the observation weights are normalized such that their sum equals the prior class probability, which is stored in the *Prior* attribute of the kNN classification model. As a result, $\sum_{j=1}^{m} w_j = 1$. Generally, a lower classification loss implies a more accurate and effective predictive model, and we do in fact observe that the classification loss decreases as the gait cycle progresses. A classification loss below 10% for window 6, although not followed by an increased accuracy, suggests that the classifier has strong generalization to new data (Fig. 3).

Additionally, the kNN classifiers in our system effectively distinguish between surfaces with widely differing stiffness levels, such as transitions from rigid (R) to low-stiffness (TL) surfaces. However, we observed more frequent misclassifications in cases like transitions between rigid (R) and high-stiffness (TH) surfaces (see Fig. 3). This is likely due to the similar nature of these surfaces, which presents a greater challenge for accurate classification. Finally, comparing our framework with a random choice classifier that would on average yield a 25% prediction accuracy, we can confidently say the results of this work are particularly encouraging for the application of our framework in powered prostheses.

B. Naive Bayes enhanced the overall prediction accuracy

The classification results for each segmented window produced highly encouraging predictions, with our TT participant achieving an accuracy of 76.2%. By incorporating Naive Bayes as a cumulative step in our framework, we were able to boost classification accuracy by 6.8% (83% accuracy) when all six windows were included, by 4.8% (81% accuracy) when the first five windows were used, and by 2.8% (79% accuracy) when the first three or four windows were employed, allowing us to make a timely prediction about 225ms before the actual surface transition and tune the prosthesis controller parameters accordingly (see Fig. 4). An example of a possible control action for the prosthesis could be the adjustment of impedance or ankle stiffness. Given the current computational power of micro-controllers usually found in lower limb prostheses, this time is enough to alter the prosthesis's control parameters to safely accommodate such transitions. The success of this framework lies thus within its ability to predict the transitions between surfaces of variable stiffness before they happen, i.e., before the foot of the user lands on the new surface.

IV. Discussion

This study demonstrates the feasibility of classifying and predicting surface compliance for individuals with transtibial lower-limb amputation (TT LLA) using electromyographic (EMG), kinematic, and kinetic data. Our framework significantly outperforms a random choice classifier, which would yield only 25% accuracy, underscoring its potential for improving the control architecture of powered lower-limb prostheses.

To enhance the generalizability of our approach, future work will include testing with more individuals with TT LLA and will focus on extending our study to real-world terrains beyond VST 2, which provided a controlled and repeatable testing environment. Capturing the complexities of natural soft surfaces will enable a more comprehensive evaluation of the robustness of our system. Additionally, recognizing the challenges of obtaining knee and hip kinematics in real-world applications, particularly for individuals with LLA, our aim is to explore alternative sensing strategies. Inertial Measurement Units (IMUs) and other biomechanical sensing methods will be investigated to provide equivalent insights while maintaining real-world applicability.

By addressing these aspects, we move closer to developing a robust, real-time control framework for powered prostheses that adapts to diverse terrains, ultimately improving mobility and quality of life for prosthesis users.

V. Conclusion

The results of this study as the first attempt to classify and predict surface compliance in TT LLA population are particularly significant. By combining EMG signals with kinematic, and kinetic data, the proposed system was able to accurately differentiate between the user's intent to step on surfaces of rigid, high, medium, or low stiffness, encompassing a broad spectrum of real-world environments. In this work, we successfully tested this algorithm with the clinical population and acquired results comparable to our previous studies with healthy subjects [15].

Our framework can be integrated into the prosthesis high-level control and enable real-time adjustments to prostheses or lower extremity devices based on user intent. Considering the need for transparent shared control between the user and the prosthesis that will anticipate the required ankle kinematics and dynamics, and react to the environmental stimuli our framework aims to 1) increase the overall efficiency and robustness of lower limb prosthetic and wearable devices, and 2) lower the cognitive burden on the users by allowing the feedback controller to handle commonly needed corrective responses. This innovation could improve the reliability and safety of lower-limb prosthetics and wearable devices, ultimately enhancing the quality of life for individuals with gait impairments, including those with LLA.

VI. Acknowledgments

We would like to thank Independence Prosthetics-Orthotics Inc., who is part of the Eqwal group, for assistance with participant recruitment.

References

[1] X. Wang, N. O'Dwyer, and M. Halaki, "A review on the coordinative structure of human walking and the application of principal component analysis," *Neural Regeneration Research*, vol. 8, p. 662, 3 2013.

[2] M. D. Chang, E. Sejdić, V. Wright, and T. Chau, "Measures of dynamic stability: Detecting differences between walking overground and on a compliant surface," *Human movement science*, vol. 29, no. 6, pp. 977–986, 2010.

[3] M. J. MacLellan and A. E. Patla, "Adaptations of walking pattern on a compliant surface to regulate dynamic stability," *Experimental brain research*, vol. 173, pp. 521–530, 2006.

[4] D. S. Marigold and A. E. Patla, "Adapting locomotion to different surface compliances: Neuromuscular responses and changes in movement dynamics," *Journal of Neurophysiology*, vol. 94, no. 3, pp. 1733–1750, 2005.

[5] B. J. Hafner, S. J. Morgan, D. C. Abrahamson, and D. Amtmann, "Characterizing mobility from the prosthetic limb user's perspective: Use of focus groups to guide development of the prosthetic limb users survey of mobility," *Prosthetics and Orthotics International*, vol. 40, pp. 582–590, 10 2016.

[6] J. Kim, M. J. Major, B. Hafner, and A. Sawers, "Frequency and circumstances of falls reported by ambulatory unilateral lower limb prosthesis users: A secondary analysis," *Physical Medicine and Rehabilitation*, vol. 11, pp. 344–353, 4 2019.

[7] S. J. Morgan, B. J. Hafner, and V. E. Kelly, "Dual-task walking over a compliant foam surface: A comparison of people with transfemoral amputation and controls," *Gait & Posture*, vol. 58, pp. 41–45, 2017.

[8] N. Arifin, N. A. Abu Osman, S. Ali, H. Gholizadeh, and W. A. B. W. Abas, "Postural stability characteristics of transtibial amputees wearing different prosthetic foot types when standing on various support surfaces," *TheScientificWorldJournal*, vol. 2014, p. 856279, 2014.

[9] J. Carpentier and P.-B. Wieber, "Humanoid and bipedal robotics (e yoshida, section editor) recent progress in legged robots locomotion control," *Current Robotics Reports*, 2021.

[10] S. E. Davies and S. N. Mackinnon, "The energetics of walking on sand and grass at various speeds," *Ergonomics*, vol. 49, pp. 651–660, 6 2006.

[11] C. Hennah and M. Doumas, "Dual-task walking on real-world surfaces: Adaptive changes in walking speed, step width and step height in young and older adults," *Experimental gerontology*, vol. 177, 6 2023.

[12] M. E. V. den Berg, C. J. Barr, J. V. McLoughlin, and M. Crotty, "Effect of walking on sand on gait kinematics in individuals with multiple sclerosis," *Multiple Sclerosis and Related Disorders*, vol. 16, pp. 15–21, 8 2017.

[13] C. Karakasis, R. Salati, and P. Artemiadis, "Adjusting the quasi-stiffness of an ankle-foot prosthesis improves walking stability during locomotion over compliant terrain," *IEEE International Conference on Intelligent Robots and Systems*, pp. 2140–2145, 2023.

[14] B. Hobbs and P. Artemiadis, "Virtual reality-based robot-assisted method for gait training showing retention of anticipatory motor responses," in *10th IEEE RAS/EMBS International Conference on Biomedical Robotics and Biomechatronics (BioRob)*, 2024.

[15] C. Angelidou and P. Artemiadis, "On predicting transitions to compliant surfaces in human gait via neural and kinematic signals," *IEEE Transactions on Neural Systems and Rehabilitation Engineering*, vol. 31, pp. 2214–2223, 2023.

[16] V. Chambers and P. Artemiadis, "Using robot-assisted stiffness perturbations to evoke aftereffects useful to post-stroke gait rehabilitation," *Frontiers in robotics and AI*, vol. 9, 1 2023.

[17] C. Angelidou and P. Artemiadis, "On predicting transitions to compliant surfaces in human gait via neural and kinematic signals," *IEEE Transactions on Neural Systems and Rehabilitation Engineering*, vol. 31, pp. 2214–2223, 2023.

[18] C. Angelidou and P. Artemiadis, "On intuitive control of ankle-foot prostheses: A sensor fusion-based algorithm for real-time prediction of transitions to compliant surfaces," *2023 IEEE/RSJ International Conference on Intelligent Robots and Systems (IROS)*, pp. 2122–2127, 10 2023.

[19] C. Angelidou and P. Artemiadis, "Reducing complexity, enhancing precision: Predicting compliant surface transitions in walking via neighborhood component analysis," in *10th IEEE RAS/EMBS International Conference on Biomedical Robotics and Biomechatronics (BioRob)*, 2024.

[20] D. P. Henson, C. Edgar, Z. Ding, B. Sivapuratharasu, P. L. Feuvre, M. E. Finnegan, R. Quest, A. H. McGregor, and A. M. Bull, "Understanding lower limb muscle volume adaptations to amputation," *Journal of Biomechanics*, vol. 125, 8 2021.

[21] V. Chambers, B. Hobbs, W. Gaither, A. Zhou, C. Karakasis, and P. Artemiadis, "The variable stiffness treadmill 2: Development and validation of a unique tool to investigate locomotion on compliant terrains," *Journal of Mechanisms and Robotics*, vol. 17, no. 3, 2025.

[22] Vicon Motion Systems, "Plug-in gait reference guide," https://help.vicon.com/space/Nexus216/11607059/Plug-in+Gait+Reference+Guide.

[23] H. J. Hermens, B. Freriks, C. Disselhorst-Klug, and G. Rau, "Development of recommendations for semg sensors and sensor placement procedures," *Journal of Electromyography and Kinesiology*, vol. 10, pp. 361–374, 10 2000.

[24] D. F. Stegeman, B. U. Kleine, B. G. Lapatki, and J. P. Van Dijk, "High-density surface emg: Techniques and applications at a motor unit level," *Biocybernetics and biomedical engineering*, vol. 32, no. 3, pp. 3–27, 2012.

[25] G. Wang, Q. Li, L. Wang, W. Wang, M. Wu, and T. Liu, "Impact of sliding window length in indoor human motion modes and pose pattern recognition based on smartphone sensors," *Sensors 2018, Vol. 18, Page 1965*, vol. 18, p. 1965, 6 2018.

[26] W. Yang, K. Wang, and W. Zuo, "Neighborhood component feature selection for high-dimensional data," *Journal of Computers*, vol. 7, pp. 162–168, 2012.

[27] G. F. M. de Souza, A. C. Netto, A. H. de Andrade Melani, M. A. de Carvalho Michalski, and R. F. da Silva, "Engineering systems' fault diagnosis methods," *Reliability Analysis and Asset Management of Engineering Systems*, pp. 165–187, 2022.